Journal of Atmospheric and Solar-Terrestrial Physics 130-131 (2015) 151–158

Contents lists available at ScienceDirect

Journal of Atmospheric and Solar-Terrestrial Physics

journal homepage: www.elsevier.com/locate/jastp

Research Paper

Plasma bubble monitoring by TEC map and 630 nm airglow image

H. Takahashi [a,*], C.M. Wrasse [a], Y. Otsuka [b], A. Ivo [a], V. Gomes [a], I. Paulino [c], A.F. Medeiros [c], C.M. Denardini [a], N. Sant'Anna [a], K. Shiokawa [b]

[a] EMBRACE, Instituto Nacional de Pesquisas Espaciais, São José dos Campos, SP, Brazil
[b] STEL, Nagoya University, Nagoya, Japan
[c] Universidade Federal de Campina Grande, Campina Grande, PB, Brazil

ARTICLE INFO

Article history:
Received 5 December 2014
Received in revised form
24 April 2015
Accepted 7 June 2015
Available online 11 June 2015

Keywords:
Plasma bubbles
TEC mapping
Optical imaging
Solar terminator

ABSTRACT

Equatorial ionosphere plasma bubbles over the South American continent were successfully observed by mapping the total electron content (TECMAP) using data provided by ground-based GNSS receiver networks. The TECMAP could cover almost all of the continent within ~4000 km distance in longitude and latitude, monitoring TEC variability continuously with a time resolution of 10 min. Simultaneous observations of OI 630 nm all-sky image at Cachoeira Paulista (22.7°S, 45.0°W) and Cariri (7.4°S, 36.5°W) were used to compare the bubble structures. The spatial resolution of the TECMAP varied from 50 km to 1000 km, depending on the density of the observation sites. On the other hand, optical imaging has a spatial resolution better than 15 km, depicting the fine structure of the bubbles but covering a limited area (~1600 km diameter). TECMAP has an advantage in its spatial coverage and the continuous monitoring (day and night) form. The initial phase of plasma depletion in the post-sunset equatorial ionization anomaly (PS-EIA) trough region, followed by development of plasma bubbles in the crest region, could be monitored in a progressive way over the magnetic equator. In December 2013 to January 2014, periodically spaced bubble structures were frequently observed. The longitudinal spacing between the bubbles was around 600–800 km depending on the day. The periodic form of plasma bubbles may suggest a seeding process related to the solar terminator passage in the ionosphere.

1. Introduction

The equatorial ionosphere suffers serious modifications during the period from sunset to evening. During astronomical twilight conditions, the solar terminator passes through the ionosphere and ionization ceases. Under the presence of zonal winds in the lower thermosphere, pre-reversal **ExB** uplifting of the ionosphere produces amplification of plasma density in the off-equatorial latitudes, forming the post-sunset equatorial ionization anomaly (PS-EIA) (Rishbeth, 2000). The quick uplift also contributes to a condition of plasma instability (Rayleigh–Taylor instability), which triggers plasma depletions (bubbles) under certain physical conditions (Kelley, 2009). Characteristics of the bubbles such as temporal evolutions, vertical and latitudinal development and longitudinal variability have been studied extensively using different techniques (e.g., Sobral et al., 2002; Burke et al., 2004; Nishioka et al., 2008; Dao et al., 2011; Carter et al., 2013). However, clarification of the conditions of plasma bubble seeding is still a scientific concern as pointed out by Retterer and Roddy (2014). Atmospheric gravity wave induced F-layer perturbation could be one explanation (e.g., Abdu et al., 2009). Presence of large scale wave structures (LSWS) during the post-sunset period could be another triggering process (Tsunoda et al., 2011).

One of the difficulties in advancing the discussion of the plasma bubble seeding process is a limitation of bubble monitoring in a sufficiently large two-dimensional area. An all-sky imager of OI 630 nm emission can produce two-dimensional bubble images within a diameter of ~1600 km, corresponding to approximately 15° of longitude. The advantage of optical imaging is its spatial resolution (approximately 15 km), which makes it possible to observe the fine structure of the bubble (Takahashi et al., 2009). However, it is difficult to cover a wider range. Ogawa et al. (2005) used two imagers to cover the geomagnetic conjugate points with a distance of 5400 km. Recent work by Makela et al. (2010) covered a large longitudinal range from the off-equatorial observation site. This was possible, however, only when the bubbles were well developed vertically and elongated to the low-to-middle latitudes along the magnetic field line. Another limitation of airglow measurements would be dependence on favorable weather conditions.

Recent development of the total electron content (TEC) measurement by ground-based GNSS receivers has made observations achievable over a large area. Valladares et al. (2004) mapped TEC

* Corresponding author.
E-mail address: hisao.takahashi@inpe.br (H. Takahashi).

http://dx.doi.org/10.1016/j.jastp.2015.06.003
1364-6826/

along the meridian using GNSS receivers strategically distributed along the western coast of South America. Takahashi et al. (2014) presented TEC in the two-dimensional form over Brazil and showed development of PS-EIA. Large-scale TEC depletions parallel to the magnetic field lines were also detected. GNSS based TEC measurement is, however, dependent on the density of the ground receiver network. Otsuka et al. (2013) mapped the medium-scale traveling ionospheric disturbances (MSTIDs) over Europe using dense ground-based receiver sites. Simultaneous observation of the ionospheric irregularities using TEC mapping and OI 630 nm images have been successfully conducted by Saito et al. (2001). They were able to make a MSTID map using optical imagers and a dense GPS receiver network data. Simultaneous optical and radio wave measurement of plasma bubbles made it possible to monitor wave structures in a more detailed form. Recently, Haase et al. (2011) observed plasma depletions by OI 630 nm airglow imager and groundbased GPS receivers and compared the depletion characteristics obtained by the two techniques. They reported that the two techniques are useful for observing the time and latitudinal evolution of the depletions.

There are three main GNSS receiver networks on the South American continent, as mentioned in the next section. Using more than 130 ground receivers in total, we plot TEC and attempt to make TEC maps over South America. The spatial resolution varies depending on the density of the receivers. During the nighttime, we also obtained OI 630 nm optical imaging data. Two techniques therefore complement each other to map the ionospheric irregularities in two-dimensional forms. In the present work, therefore, we demonstrate the ionosphere TEC map (hereafter TECMAP) over South America and study plasma bubble structures simultaneously observed by the GNSS receiver network and optical imagers. At the end of December 2013, on several occasions, we observed periodically spaced plasma bubbles appeared in the central part of the continent and propagating eastward. A possible generation process of such bubble structures will be discussed.

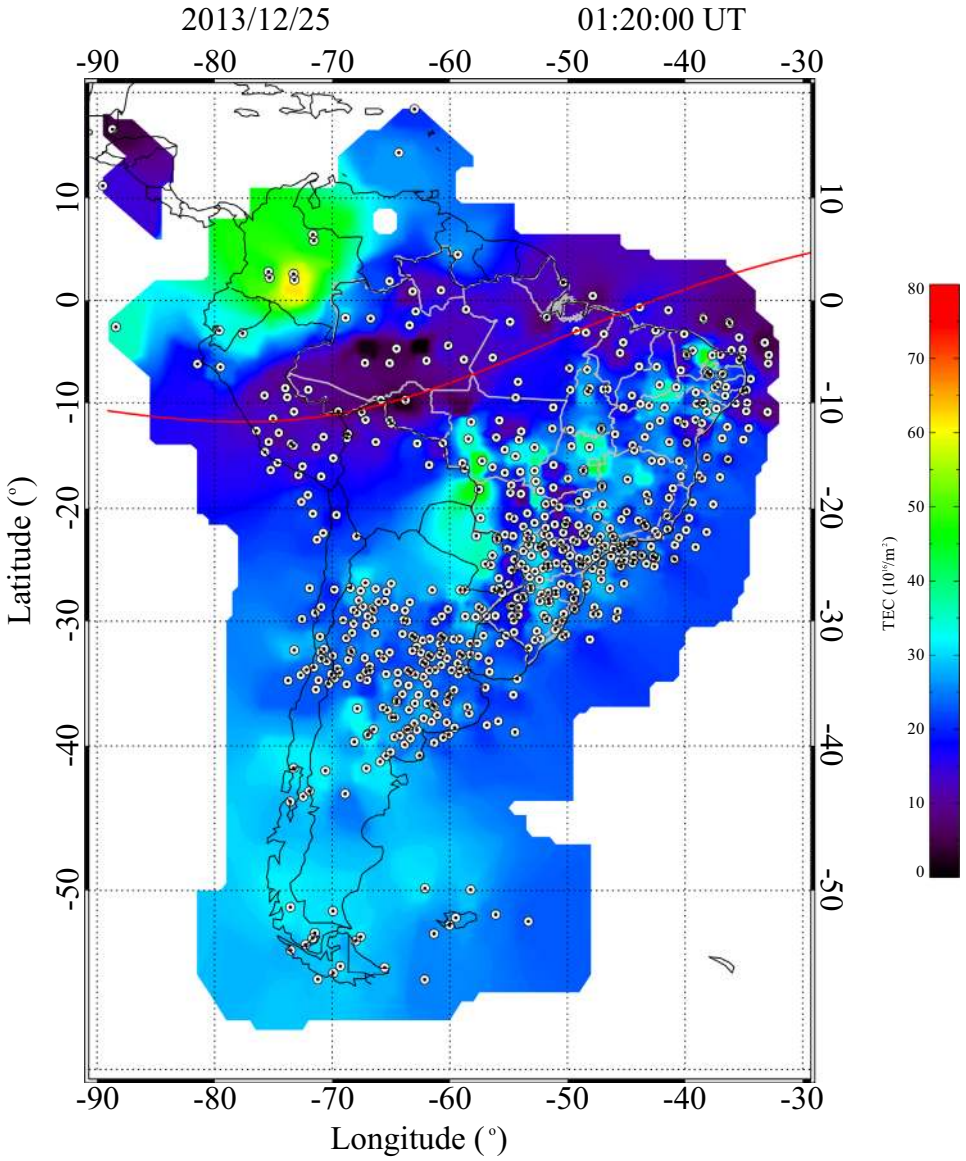

Fig. 1. GNSS based TEC observation points (ionospheric pierce points) over South America on the night of December 24–25, 2013, at 01:20 UT. The color shade presents TECu from 1(purple) to 80(red). The red line indicates the geomagnetic equator.

2. Observation and data analysis

2.1. GPS TEC observation

Ground-based dual frequency GNSS receivers have been operated by IBGE (Brazilian Institute for Geography and Statistics). IBGE releases a package of RINEX format data (RBMC) from approximately 90 sites throughout Brazil, with 10 min time intervals (IBGE website, 2014). In addition to the RBMC data, the data from IGS (International GNSS Service) (IGS website, 2013), LISN (Low latitude Ionospheric Sensor Network) (LISN website, 2014) and RAMSAC (Red Argentina de Monitoreo Satelital Continuo) (RAMSAC website, 2014) were also collected and processed. In this way, all of Brazil, Peru, Chile and Argentina were covered. No ground-based sites were available from the central part of South America (Bolivia and Paraguay). The total number of ground-based receivers over the entire continent was approximately 130. Normally, one receiver looks up four to six GPS satellites simultaneously. In the present work, GPS transmitting waves with an elevation angle higher than 30° were used. Therefore, a relatively high density of TEC observations could be achieved. Fig. 1 presents the observation points (ionospheric pierce point between ground receiver and GPS satellite) over South America at 01:20 UT, December 25, 2013. The pierce points are obtained by assuming the ionospheric peak height to be 300 km altitude (Otsuka et al., 2013). The total number of observation points was 646. One can notice that there is a relatively high-density observation area (20°–30°S and 40°–60°W) where better spatial resolution (50–150 km) can be achieved. However, less observation points were available in the equatorial region (mainly Amazon Forest) and the Northern Hemisphere low latitude regions; in some locations, there was more than 500 km of distance from one point to the next, which caused difficulties in tracking the spatial variations of TEC. No data point was available in the area of 15°–26°S and 60°–70°W.

The total electron content (TEC) along the line of sight between the GNSS satellite and a ground receiver (SlantTEC) was calculated using pseudoranges (P1 and P2) and the phase difference between the carrier waves (L1 and L2). The vertical TEC (VTEC) is obtained with SlantTEC multiplied by a slant factor. The slant factor (S) is defined as τ_0/τ_1, where τ_1 is the length of the ray path between altitudes of 250 and 450 km and τ_0 is the thickness of the ionosphere (200 km) for the zenith path. The VTEC values are therefore mapped on the ionospheric shell at a pierce point of the line of sight. The data processing procedures were based on those presented by Otsuka et al. (2002) and Takahashi et al. (2014). The vertical TEC values (VTEC) obtained in this manner are shown in Fig. 1, with shades of color representing low (dark blue) to high (TECu ~80, red) values.

TEC data were mapped on the ionospheric shell at a 300 km altitude with a horizontal cell of 0.5° × 0.5° in latitude and longitude. To optimize the spatial resolution of TEC and to cover the entire area with TEC values, we first calculated a running average of three points with a 0.5° element; this corresponds to 3 × 3 elements covering an area of ~160 km square at latitudes of 10°–20°. If no data were found in the area, the running average area expands to 5 × 5 elements, which corresponds to approximately 260 km square. In this way, the running average element expands up to 21 × 21 elements, which corresponds to 1090 km square as the extreme case. Therefore, the spatial resolution of the TEC map varies depending on the number of sites entered in the area in concern. On average, the spatial resolution is approximately 100 km in the southeastern part of Brazil, 200–300 km in the northeastern part and greater than 500 km in the Amazon region and the central part of the continent.

TECMAP in Fig. 1 depicts large latitudinal and longitudinal variations of TEC along the magnetic equator; it varies from a few TECu in the equatorial region to ~50 TECu in the low to middle latitudes. The green to yellow belt is extended over the latitudinal range from (10°S, 35°W) to (35°S, 60°W). A similar green to yellow belt is extended in the Northern Hemisphere from (10°N, 60°W) to (0°S, 80°W). These plasma enhancements are due to the equatorial ionization anomaly after sunset (PS-EIA). The low intensity of TEC (blue) along the magnetic equator is the plasma density trough generated by the PS-EIA. The geomagnetic equator is shown in the figure (red line). One can recognize that low TEC belts penetrate into the plasma crest region at approximately 38°W, 43°W and 52°W, forming plasma depletion belts. These are most likely plasma bubble signatures, which will be discussed later. However, no clear signature of the depletion belts can be observed in the Northern Hemisphere. This is due to a lack of observation points in this area, resulting in low spatial resolution.

2.2. Optical imaging of OI 630 nm emission

Two all-sky imagers, with a 180° wide-angle fish-eye lens, followed by a telecentric lens system and narrow band optical filters, have been used to obtain a monochromatic image on a CCD camera. One imager was installed at Cariri airglow observatory in the equatorial region (7.4°S, 36.5°W), and the other was operated at Cachoeira Paulista (22.7°S, 45.0°W). For the present study, two optical filters were used to measure the airglow OI 630 nm and OHNIR (715–930 nm). The exposure time to take an image was 90 s for OI 630 nm and 15 s for OHNIR. The 630 nm image covers a horizontal extension of 1600 km (at the zenith angle of 75°) at an altitude of 250 km, permitting the image to cover the latitudinal and longitudinal extension of the plasma depletions along the magnetic field line.

Fig. 2(A) presents a flat-field image of OI 630 nm emission taken at Cachoeira Paulista on the night of February 01, 2014, at 00:30 UT. The brightness of the emission is shown by a normalized gray scale. The image shows a dark belt (depletion of the emission rate) extending from the north to the south direction centered at around 45°W. This is a footprint of plasma bubbles in the 630 nm emission layer at approximately 250 km altitude. The overhead zonal width of the bubble is approximately 220 ± 20 km. Inside the large extended bubble, one can see a fine structure of bifurcation. To compare it with TEC depletion, TECMAP is also shown in Fig. 2(B). The depletion form is similar to that of the 630 nm bubble. The center of the depletion, however, is slightly dislocated by approximately one degree (~100 km) westward compared to the 630 nm bubble. It should be noted that the two techniques look the depletion at different altitudes. TECMAP depicts the depletion over the 250–450 km altitude range as assumed in the TEC calculation. On the other hand, the 630 nm image projects the bubble at around 250 km altitude. The longitudinal difference of the two depletions might indicate that the bubble is tilted westward with increasing height. The westward tilting structures have been reported by several authors (e. g., Makela and Kelley, 2003; Haase et al., 2011). However, a possibility of an error in the longitudinal difference caused by the altitude designations between the two methods cannot be ruled out. The high TEC zone in the TECMAP (a light green to yellow belt in Fig. 2(B)) coincides with the high intensity brightness of the 630 nm image. Although there is a difference in some detail between image and TECMAP, it looks to be evident that the two tools are observing a same ionospheric plasma bubble. Besides, it is clear that the OI 630 nm imager presents a better spatial resolution than TECMAP in the present case.

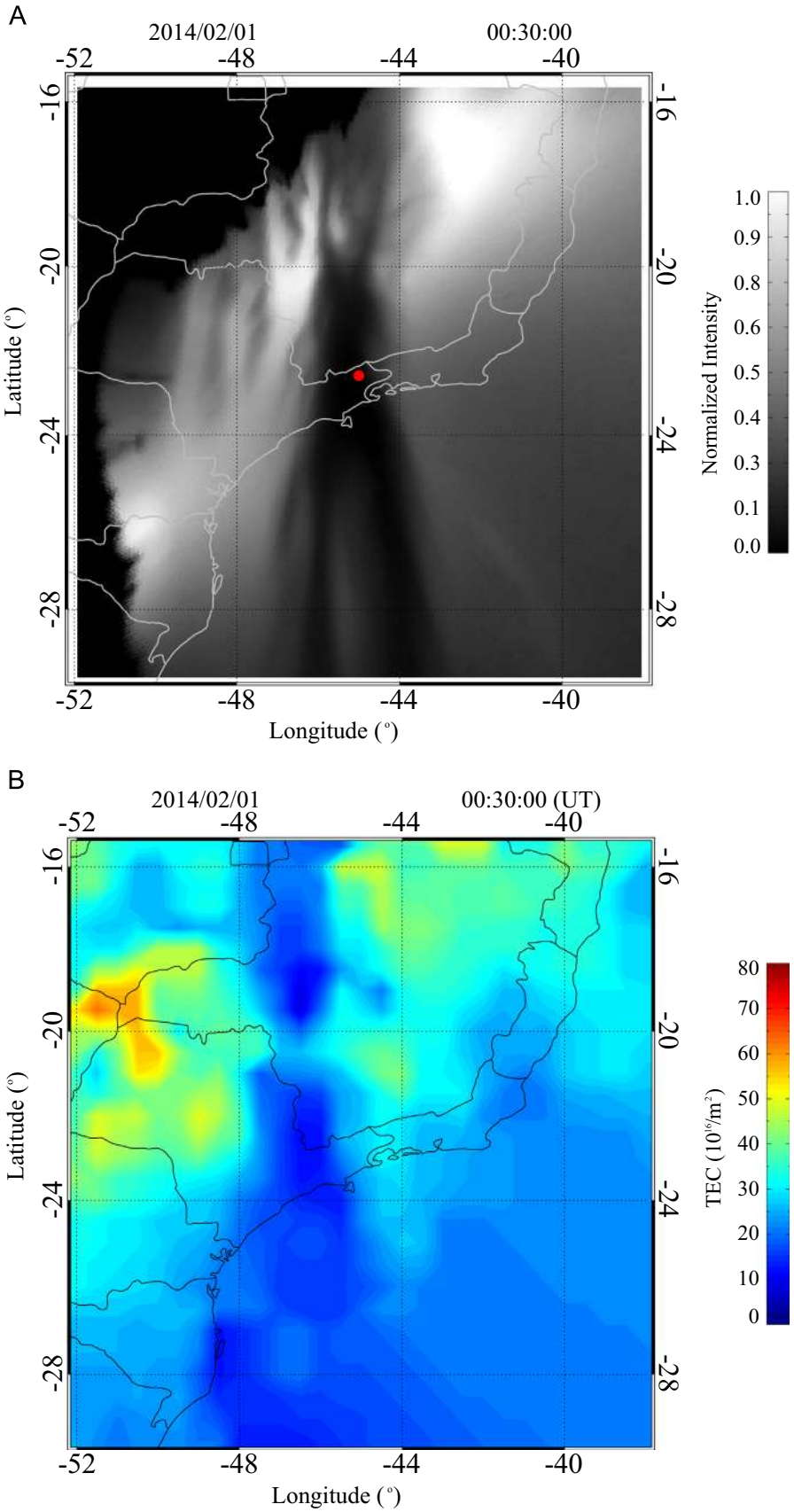

Fig. 2. (A) Flat field OI 630 nm all-sky image (left hand side) at Cachoeira Paulista (22.7S, 45.0W). The gray scale is a normalized emission rate. Red dot indicates the location of observatory. (B) TECMAP (right hand side) over the southeastern area of Brazil. Both were taken on the night of February 01, 2014, at 00:30 UT.

3. Results

3.1. Characteristics of plasma bubbles

To follow the plasma bubble formation and progress by TECMAP, three snapshots at 22:30 UT, 23:00 UT and 23:40 UT on the night of December 24–25 are shown in Fig. 3. In this way, bubble formations and the eastward drifting features can be monitored in the two dimensional form. At 22:30 UT (Fig. 3(A)), there are two depletions located at 40°W and 46°W in the latitudinal zone from 5° to 10°S. The first one at 40°W seems to be a bubble developed earlier, and the second one (46°W) is in a developing phase. This is much clearer to see in the map at 23:00 UT (Fig. 3(B)), where the second one became a more depleted form. It can be noticed that another depletion is starting to form at around 52°W. As the twilight is progressing westward, the equatorial plasma trough shows a periodic depletion form, as can be seen at 23:40 UT (Fig. 3 (C)). The distance between the depletions is around 670($\pm$ 20) km.

Optical keograms (zonal and meridional) of the 630 nm images observed at Cariri on this night are shown in Fig. 4. Slit images cutting the all-sky images in the east–west (north–south) direction passing over the local zenith are plotted as a function of time for the zonal (meridional) keogram. The emission rate is normalized. The observation stopped at 02:00 UT (December 25) because the sky condition became cloudy. Plasma bubbles (dark belts) passing over the observation site can be noticed. Several (at least 3) bubbles at around 23:00 UT can be seen both in the zonal (top) and meridional (bottom) cuts. Unfortunately these short period ($\sim$15 min) bubble structures cannot be seen in the TECMAP. The spatial resolution of the TECMAP over this region (5–10°S) is low (150–200 km). On the other hand, the wide and long extended bubble at around 00:20 UT in the keogram can be seen in the TECMAP (Fig. 3(C), at 40°W). From the horizontal gradient of the zonal component in the keogram, the longitudinal drift velocity can be estimated to be 159 $\pm$ 10 m/s. From the TECMAP bubble drifting mode, we also estimate the zonal drift velocity of 153 $\pm$ 15 m/s. Although the zonal drift velocities obtained by the two methods are in agreement in the error ranges, the former is slightly higher than the latter by $\sim$6 m/s. This might explain the westward tilting structure explained in the previous section (Fig. 2).

Also shown in the TECMAPs (Fig. 3) is the progress of the astronomical twilight zone (white dotted lines). The Earth's shadow height in this case is at approximately 300 km altitude. There

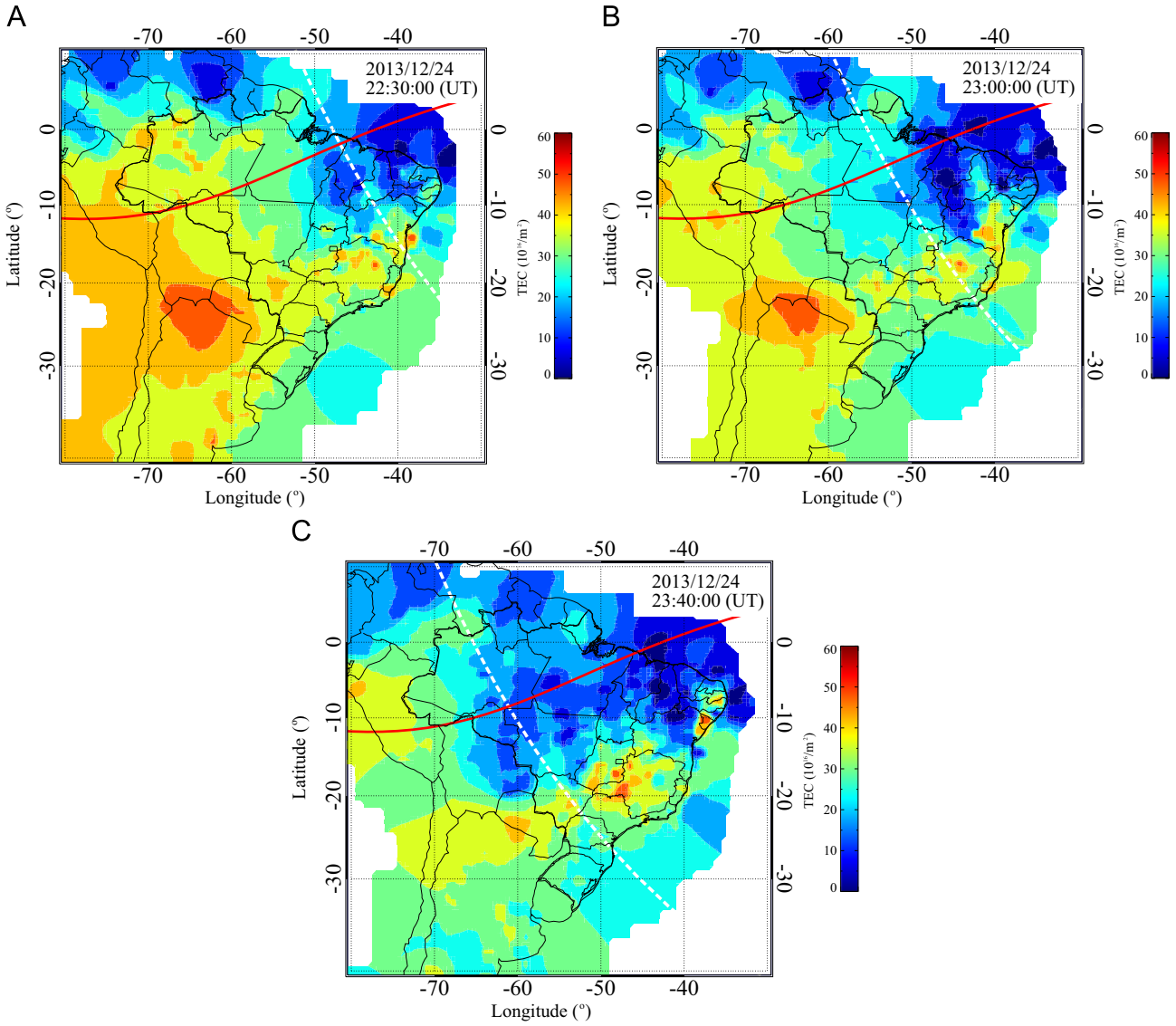

Fig. 3. (A)–(C) TECMAP at 22:30, 23:00 and 23:40 UT, respectively, on the night of December 24–25, 2013. The white lines indicate the solar terminator at 300 km altitude. The red line is the geomagnetic equator.

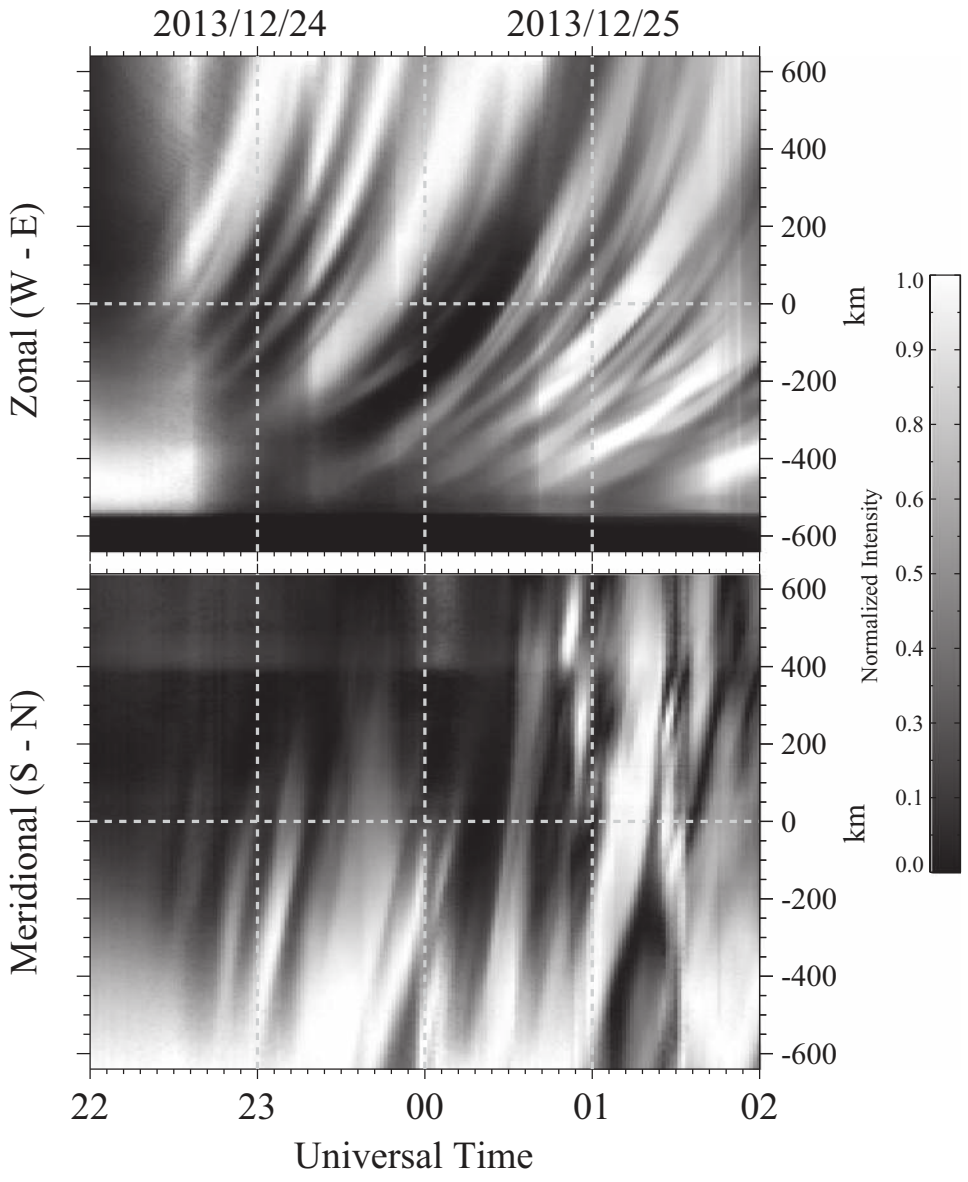

Fig. 4. Keogram of OI 630 nm airglow image in the night of December 24–25, 2013. The top image is zonal cut and the bottom is meridional cut. The gray scale is a normalized emission rate.

appears to be a large TEC gradient around the twilight line; this is because, in addition to the PS-EIA progress, the ionization process ceased when the Earth's shadow reached higher than 100 km altitude. According to Liu et al. (2009), there must be a drastic change in the thermospheric density and temperature during the terminator passage. Large TEC depletion against the progress of the twilight line observed in the present case could be partly due to the similar effect.

3.2. Periodic spacing bubble structures

After 01:00 UT (December 25), the plasma bubbles over the continent formed a structure with periodic spacing. Fig. 5 shows the TECMAP sequence from 01:00 to 02:00 UT. At least five bubbles (named B1–B5 in the figure) can be recognized at 02:00 UT (Fig. 5(C)). Some of the depletions in the figures, however, are not homogeneous. This is partly due to the optimized running average process adopted. The distance between them is almost constant at approximately 660 ± 20 km. The periodically spaced bubble structure started at 01:00 UT and continued until 04:00 UT. The spacing is almost same to those observed before 00:00 UT, suggesting that these are fossil of which developed in the early evening.

4. Discussion

Using two different tools, radio wave and optical imaging, we successfully observed the equatorial plasma bubbles over the South American continent. The optical imaging of the 630 nm emission provides detail of the longitudinal structure of the bubbles, such as multi-structures and/or bifurcations with the spatial resolution of $\sim$15 km. It appears that there are several fine structures imbedded in a large extended bubble, as seen in Fig. 4. TEC mapping provides large-scale coverage of plasma bubbles, although the spatial resolution is dependent on the density of the observations site and pierce points in the ionosphere. One can notice that the spatial resolution is high, less than 100 km, in the region of 45–55°W by 20–30°S. However, the resolution is low, longer than 300 km, in the equatorial to low latitude regions (50–

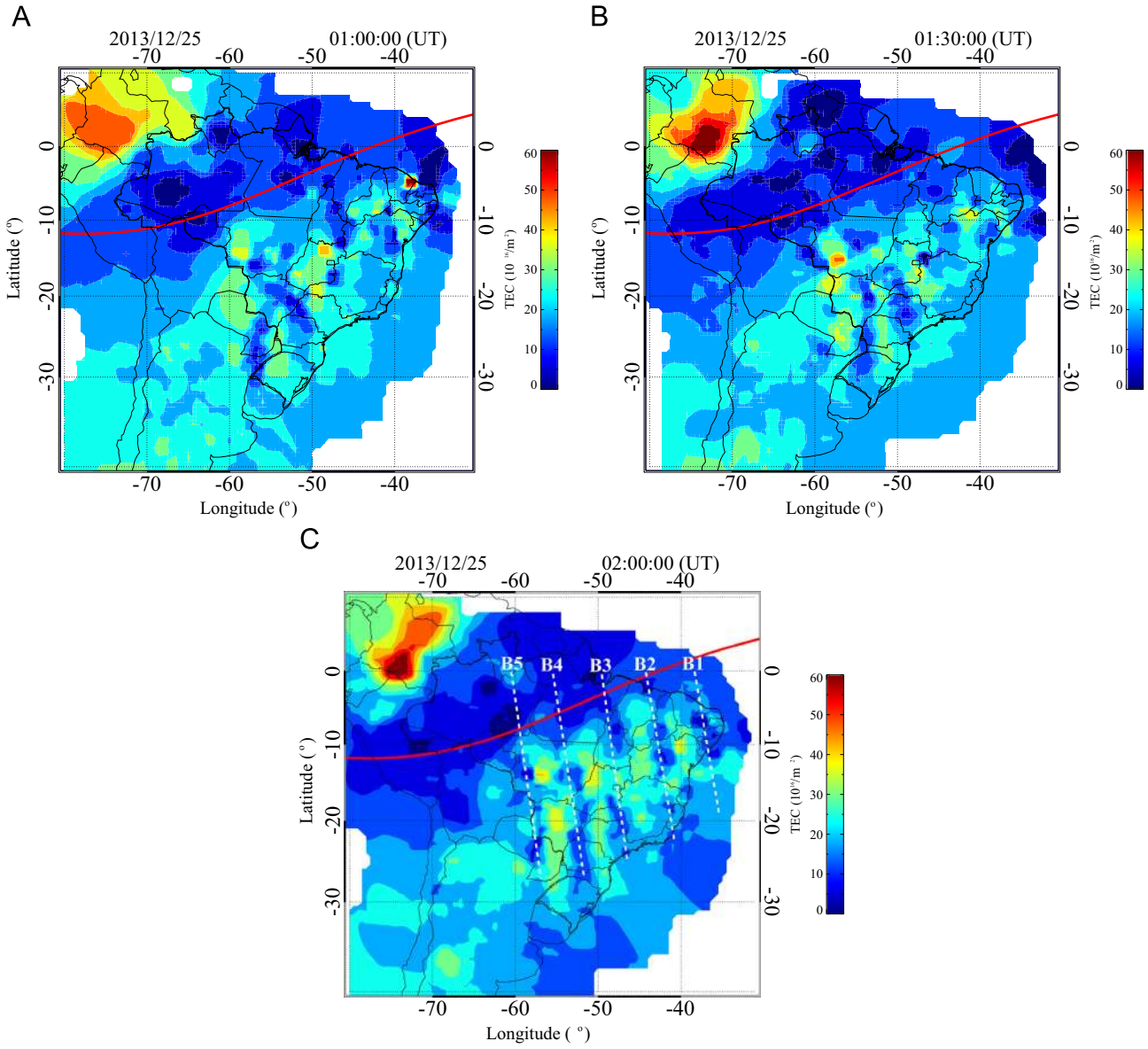

Fig. 5. (A)–(C) TECMAP at 01:00, 01:30 and 02:00 UT, respectively, on the night of December 24–25, 2013. The red line indicates the geomagnetic equator, The dashed lines (B1–B5) in the 02:00 UT map indicate the bubble locations along the longitude.

70°W by 0–10°S). Nevertheless, the time resolution of 10 min and the ability to observe continuously (24 h) are a great advantage of this technique, which is an important factor for ionospheric weather monitoring.

Plasma bubble monitoring by TEC mapping technique has also been successfully carried out by Valladares et al. (2004). They mapped TEC depletion and GPS scintillations as a function of latitude and time. In total 9 ground-based GPS receivers, located along the magnetic meridian over the ~70°W zone, were used. Our present work extended their observation covering TECMAP longitudinally by more than 3000 km. This made it possible to monitor several bubbles simultaneously: the latitudinal development and longitudinal distributions.

The most striking feature is that the present TECMAP was able to monitor the initial phase of the equatorial trough, followed by generation of plasma bubbles. The distance of the bubbles was around 600–900 km depending on the day. It would be worthwhile to further investigate the periodically spaced plasma bubbles. Makela et al. (2010) showed similar periodic spacing (200–600 km) between the bubbles observed away from the magnetic equator (30°S, geomag. 17°S). Huang et al. (2013) also observed quasi-periodic plasma bubbles by C/NOFS satellite over the African and Asian sectors. The plasma bubbles were generated in the evening sector after sunset with a period of 15–30 min and a longitudinal separation of 500–1000 km. Our present results are similar to their observations.

The periodically spaced bubble structures would suggest to us a certain specific seeding process. Abdu et al. (2009) observed periodic oscillation (20–60 min) of the F-layer bottom side density perturbations, 1–2 h prior to the sunset, and then observed plasma bubbles. Horizontal scale of the perturbation, estimated by their vertical phase propagation mode, was around 250 km. They concluded that the oscillations are due to passage of large scale gravity waves in the F-layer bottom height. Thampi et al. (2009) also observed the occurrence of large scale wave structure (LSWS) prior to the ionospheric sunset and subsequent plasma bubble occurrence by using the C/NOFS satellite data. The LSWS horizontal scale was 500–700 km. Both the authors reported that periodic oscillations in the

ionosphere prior to the ionospheric sunset have an important role to generate the plasma bubbles. From our present data analysis, however, it was not possible to investigate whether there is any plasma density oscillation before the sunset. It would be worth to further study on it.

On the other hand, our present data showed the horizontal spacing of around 600–700 km, and at least 4–5 sequences of bubbles over the South America continent. In addition to it, we observed them on several consecutive nights during the December–January period. This would suggest that the seeding process might be daily-generated by a regular form. The solar terminator twilight line could be one of the possible causes as suggested by Huang et al. (2013). They proposed that atmospheric gravity waves in the region of the sunset terminator generate the Rayleigh–Taylor instability in the F-layer, producing plasma bubbles in a periodic form. They suggest that LSWS should be a precursor of the equatorial spread F development. Tulasi Ram et al. (2014) investigated characteristics of LSWS during the sunset period and concluded that they are responsible for generating R–T instability under the condition of pre-reversal enhancement of the zonal electric field. These previous works strongly suggest that there is an atmospheric perturbation along the solar terminator that is generating ionospheric perturbations in a periodic form. Our present results also support this hypothesis. Further observational evidence, including simultaneous measurements of wind, temperature and ionospheric parameters together with TEC mapping, would help to visualize the seeding and development process of the plasma bubbles.

5. Conclusions

Ionospheric TEC maps were produced using 130 ground-based GPS receivers in South America. Simultaneously, airglow imagers produced all-sky images of the OI 630 nm emission. Both tools successfully diagnosed the spatial and temporal progress of plasma bubbles. The TEC maps provide plasma bubble structures in two-dimensional form covering more than 4000 km distance in longitude and latitude. The bubble formation and development and eastward drifting features were successfully monitored and analyzed. The optical imager provides fine structures of the bubbles, although it covers a limited area (~1600 km of diameter). The two techniques are comprehensive and useful for monitoring ionospheric irregularities. The plasma bubbles observed during the December solstice presented a periodic spacing form, which suggests a periodic seeding mechanism of the bubbles. It would be worthwhile to investigate the effect of the atmospheric density, temperature and plasma density perturbation during the passage of the solar terminator in the geomagnetic equatorial region.

Acknowledgments

The GPS ground-based receiver data were collected from the different GNSS networks in South America: RBMC of IBGE, RAMSAC from Argentina and IGS and LISN of Boston University. We are grateful to these network sites for providing the data continuously. Without their data, it would not have been possible to generate such a TECMAP. The present work was partially supported by CNPq under the Project 30.5321/2010-2.

References

Abdu, M.A., Kherani, A.E., Batista, I.S., de Paula, E.R., Fritts, D.C., Sobral, J.H.A., 2009. Gravity wave initiation of equatorial spread F/plasma bubble irregularities based on observational data from the SpreadFEx campaign. Ann. Geophys. 27, 2607–2622.

Burke, W.J., Gentile, L.C., Huang, C.Y., Valladares, C.E., Su, S.Y., 2004. Longitudinal variability of equatorial plasma bubbles observed by DMSP and ROCSAT-1. J. Geophys. Res. 109, A12301. http://dx.doi.org/10.1029/2004JA010583.

Carter, B.A., Zhang, K., Norman, R., Kumar, V.V., Kumar, S., 2013. On the occurrence of equatorial F-region irregularities during solar minimum using radio occultation measurements. J. Geophys. Res.: Space Phys. 118, 892–904. http://dx.doi.org/10.1002/jgra.50089.

Dao, E., Kelley, M.C., Roddy, P., Retterer, J., Ballenthin, J.O., de La Beaujardiere, O., Su, Y.-J., 2011. Longitudinal and seasonal dependence of nighttime equatorial plasma density irregularities during solar minimum detected on the C/NOFS satellite. Geophys. Res. Lett. 38, L10104. http://dx.doi.org/10.1029/2011GL047046.

Haase, J.S., Dautermann, T., Taylor, M.J., Chapagain, N., Calais, E., D. Pautet, D., 2011. Propagation of plasma bubbles observed in Brazil from GPS and airglow data. Adv. Space Res. 47, 1758–1776. http://dx.doi.org/10.1016/j.asr.2010.09.025.

Huang, C.-S., La Beaujardiere, O., Roddy, P.A., Hunton, D.E., Ballenthin, J.O., Hairston, M.R., Pfaff, R.F., 2013. Large-scale quasiperiodic plasma bubbles: C/NOFS observations and causal mechanism. J. Geophys. Res. 118 (6), 3602–3612. http://dx.doi.org/10.1002/jgra.50338.

IBGE website, 2014. ⟨http://www.ibge.gov.br/home/geociencias/geodesia/rbmc/rbmc_est.shtm⟩.

IGS website, 2013. ⟨http://www.igs.org⟩.

Kelley, M.C., 2009. The Earth's Ionosphere: Plasma Physics and Electrodynamics (International Geophysics Series). 96. Academic Press, San Diego, USA.

LISN website, 2014. ⟨http://lisn.igp.gob.pe⟩.

Liu, H., Hermann, L., Watanabe, S., 2009. A solar terminator wave in thermospheric wind and density simultaneously observed by CHAMP. Geophys. Res. Lett. 36, L10109. http://dx.doi.org/10.1029/2009GL038165.

Makela, J.J., Kelley, M.C., 2003. Field-aligned 777.4-nm composite airglow images of equatorial plasma depletions. Geophys. Res. Lett. 30 (8), 1442. http://dx.doi.org/10.1029/2003GL017106.

Makela, J.J., Vadas, S.L., Muryanto, R., Duly, T., Crowley, G., 2010. Periodic spacing between consecutive equatorial plasma bubbles. Geophys. Res. Lett. 37, L14103. http://dx.doi.org/10.1029/2010GL043968.

Nishioka, M., Saito, A., Tsugawa, T., 2008. Occurrence characteristics of plasma bubble derived from global ground-based GPS receiver networks. J. Geophys. Res. 113, A05301. http://dx.doi.org/10.1029/2007JA012605 2008.

Ogawa, T., Sagawa, E., Otsuka, Y., Shiokawa, K., Immel, T.I., Mende, S.B., Wilkinson, P., 2005. Simultaneous ground- and satellite-based airglow observations of geomagnetic conjugate plasma bubbles in the equatorial anomaly. Earth Planets Space 57, 385–392.

Otsuka, Y., Ogawa, T., Saito, A., Tsugawa, T., Fukao, S., Miyazaki, S., 2002. A new technique for mapping of total electron content using GPS network in Japan. Earth Planets Space 54, 63–70.

Otsuka, Y., Suzuki, K., Nakagawa, S., Nishioka, M., Shiokawa, K., Tsugawa, T., 2013. GPS observations of medium-scale traveling ionospheric disturbances over Europe. Ann. Geophys. 31, 163–172. http://dx.doi.org/10.5194/angeo-31-163-2013.

RAMSAC website, 2014. ⟨http://www.ign.gob.ar/NuestrasActividades/Geodesia/Ramsac⟩.

Retterer, J.M., Roddy, P., 2014. Faith in a seed: on the origins of equatorial plasma bubbles. Ann. Geophys. 32, 485–498. http://dx.doi.org/10.5194/angeo-32-485-2014.

Rishbeth, H., 2000. The equatorial F-layer: progress and puzzles. Ann. Geophys. 18, 730–739.

Saito, A., Nishimura, M., Yamamoto, M., Fukao, S., Kubota, M., Shiokawea, K., Otsuka, Y., Tsugawa, T., Ogawa, T., Ishii, M., Sakanori, T., Miyazaki, S., 2001. Traveling ionospheric disturbances detected in the FRONT campaign. Geophys. Res. Lett. 28 (4), 689–692. http://dx.doi.org/10.1029/2000GL011884.

Sobral, J.H.A., Abdu, M.A., Takahashi, H., Taylor, M.J., de Paula, E.R., Zamlutti, C.J., Borba, G. L., 2002. A study of the ionospheric plasma bubbles climatology over Brazil based on 22 years (1977–1998) of OI 630 nm airglow observation. J. Atmos. Terr. Phys. 64 (12–14), 1517–1524.

Takahashi, H., Taylor, M.J., Pautet, P.-D., Medeiros, A.F., Gobbi, D., Wrasse, C.M., Fechine, J., Abdu, M.A., Batista, I.S., de Paula, E., Sobral, J.H.A., Arruda, D., Vadas, S.L., Sabbas, F.S., Fritts, D.C., 2009. Simultaneous observation of ionospheric plasma bubbles and mesospheric gravity waves during the SpreadFEx Campaign. Ann. Geophys. 27, 1477–1487. http://dx.doi.org/10.5194/angeo-27-1477-2009.

Takahashi, H., Costa, S., Otsuka, Y., Shiokawa, K., Monico, J.F.G., de Paula, E., Nogueira, P., Denardini, C.M., Becker-Guedes, F., Wrasse, C.M., Ivo, A.S., Gomes, V.C.F., Gargarela Jr., W., Sant'Anna, N., Gatto, R., 2014. Diagnostics of equatorial and low latitude ionosphere by TEC mapping over Brazil. J. Adv. Space Res. 54, 385–394. http://dx.doi.org/10.1016/j.asr.2014.01.032 2014.

Thampi, S.V., Yamamoto, M., Tsunoda, R.T., Otsuka, Y., Tsugawa, T., Uemoto, J., Ishii, M., 2009. First observations of large-scale wave structure and equatorial spread F using CERTO radio beacon on the C/NOFS satellite. Geophys. Res. Lett. 36, L18111. http://dx.doi.org/10.1029/2009GL039887.

Tsunoda, R.T., Yamamoto, M., Tsugawa, T., Hoang, T.L., Ram, T.S., Thampi, S.V., Chau, H.D., Nagatsuma, T., 2011. On seeding, large-scale wave structure, equatorial spread F, and scintillations over Vietnam. Geophys. Res. Lett. 38, L20102. http://dx.doi.org/10.1029/2011GL049173.

Tulasi Ram, S., Yamamoto, M., Tsunoda, R.T., Chau, H.D., Hoang, T.L., Damtie, B., Wassaie, M., Yatini, C.Y., Manik, T., Tsugawa, T., 2014. Characteristics of large-scale wave structure observed from African and Southeast Asian longitudinal sectors. J. Geophys. Res. 119 (3), 2288–2297. http://dx.doi.org/10.1002/2013JA019712.

Valladares, C., Villalobos, J., Sheehan, R., Hagan, M., 2004. Latitudinal extension of low-latitude scintillations measured with a network of GPS receivers. Ann. Geophys. 22 (9), 3155–3175. http://dx.doi.org/10.5194/angeo-22-3155-2004.